Ava D. Segal
Center for Limb Loss and Mobility,
Department of Veterans Affairs,
1660 S. Columbian Way, MS-151,
Seattle, WA 98108
e-mail: avasegal@gmail.com

Kyle H. Yeates
Center for Limb Loss and Mobility,
Department of Veterans Affairs,
1660 S. Columbian Way, MS-151,
Seattle, WA 98108;
Department of Mechanical Engineering,
University of Washington,
Seattle, WA 98195
e-mail: kyle.yeates@gmail.com

Richard R. Neptune
Mem. ASME
Department of Mechanical Engineering,
The University of Texas at Austin,
Austin, TX 78712
e-mail: rneptune@mail.utexas.edu

Glenn K. Klute
Center for Limb Loss and Mobility,
Department of Veterans Affairs,
1660 S. Columbian Way, MS-151,
Seattle, WA 98108;
Department of Mechanical Engineering,
University of Washington,
Seattle, WA 98195
e-mail: gklute@u.washington.edu

Foot and Ankle Joint Biomechanical Adaptations to an Unpredictable Coronally Uneven Surface

Coronally uneven terrain, a common yet challenging feature encountered in daily ambulation, exposes individuals to an increased risk of falling. The foot-ankle complex may adapt to improve balance on uneven terrains, a recovery strategy which may be more challenging in patients with foot-ankle pathologies. A multisegment foot model (MSFM) was used to study the biomechanical adaptations of the foot and ankle joints during a step on a visually obscured, coronally uneven surface. Kinematic, kinetic and in-shoe pressure data were collected as ten participants walked on an instrumented walkway with a surface randomly positioned ±15 deg or 0 deg in the coronal plane. Coronally uneven surfaces altered hindfoot–tibia loading, with more conformation to the surface in early than late stance. Distinct loading changes occurred for the forefoot–hindfoot joint in early and late stance, despite smaller surface conformations. Hindfoot–tibia power at opposite heel contact (@OHC) was generated and increased on both uneven surfaces, whereas forefoot–hindfoot power was absorbed and remained consistent across surfaces. Push-off work increased for the hindfoot–tibia joint on the everted surface and for the forefoot–hindfoot joint on the inverted surface. Net work across joints was generated for both uneven surfaces, while absorbed on flat terrain. The partial decoupling and joint-specific biomechanical adaptations on uneven surfaces suggest that multi-articulating interventions such as prosthetic devices and arthroplasty may improve ambulation for mobility-impaired individuals on coronally uneven terrain. [DOI: 10.1115/1.4037563]

Keywords: multisegment foot model, kinetics, midtarsal, metatarsophalangeal, hindfoot, biomechanics

1 Introduction

Outdoor environments are replete with uneven surfaces and obstacles that increase the risk of falling. Three-quarters of falls occur outdoors, of which 75% are caused by extrinsic factors and roughly half (48%) are due to uneven surfaces [1,2]. A fall outdoors is also three times as likely to result in an injury than a fall indoors [3]. Strong evidence supports that walking on uneven surfaces challenges balance [4] with 25% of falls occurring in the coronal plane [1,5].

Several prior studies have revealed changes in coronal plane gait dynamics associated with walking on coronally uneven surfaces. For example, studies of sudden ankle inversions increased evertor muscle activations measured by surface electromyography [6–8]. Other studies demonstrated that walking on a 6–10 deg cross-slope caused a three- to five-fold increase in mediolateral ground reaction force (GRF) [9] and produced asymmetrical hip and ankle joint loading [10]. Damavandi et al. used a multisegment foot model (MSFM) to measure hindfoot–tibia and forefoot–hindfoot kinematics which revealed large coronal angular differences at the hindfoot in the first half of stance and at the forefoot in the second half of stance, indicating a partial decoupling of the foot segments to allow nonrigid conformation to the surface [11]. Others have reported increased plantar pressures at the midfoot (20%) and metatarsals (11–16%) shifted laterally when the foot was positioned upslope and shifted medially when the foot was positioned downslope, with smaller increases reported at the heel (3%) [12]. This mediolateral pressure redistribution and decoupling of the heel and forefoot implies the importance of a multisegmented foot for accommodating coronally uneven surfaces.

The foot's complex skeletal geometry and muscular architecture afford each joint the capacity to contribute to distinct mechanical roles during ambulation [13,14]. Joint torque estimates based on inverse dynamic models are a noninvasive alternative to direct measurements [8]; however, few inverse dynamic MSFMs have been developed [15–17] due to the complexities associated with isolating or estimating the forces acting on each segment [18]. Three methods have been used to estimate individual foot-segment forces during barefoot, level-ground walking that include targeting foot placement on two adjacent force plates [15], using a proportionality assumption with pressure mat measurements [16] and isolating forefoot kinetics after heel rise (terminal stance) [17]. Despite differing MSFMs and methods, these studies [15–17] each reported distinct joint kinetic contributions from each foot segment with the rigid single-segment foot model over-estimating ankle push-off power in late stance by roughly 35%. This evidence, combined with the changes in foot kinematics and muscle activation during cross-sloped walking, support the utility of a kinetic MSFM to describe potential alternations in foot joint biomechanics when negotiating coronally uneven terrain.

Manuscript received March 13, 2017; final manuscript received August 1, 2017; published online January 17, 2018. Assoc. Editor: Pasquale Vena.

The primary goal of this research was to explore hindfoot–tibia, forefoot–hindfoot and hallux-forefoot joint biomechanical adaptations when stepping on an unpredictable coronally uneven surface to improve our understanding of the foot's biomechanics during more complex tasks frequently encountered in daily ambulation. As a comparative tool, these findings may contribute to establishing design criteria for foot-ankle prostheses and orthoses and reveal the efficacy of rehabilitative interventions aimed at improving mobility on uneven terrains.

2 Methodology

2.1 Participants. Ten healthy adults (seven male, age: 44.0 ± 18.7 years, height: 1.74 ± 0.11 m, mass: 76.3 ± 15.1 kg) with no self-reported musculoskeletal or gait disorders completed the protocol. The governing Institutional Review Boards approved the study procedures, and all participants provided informed consent.

2.2 Instrumentation. A custom instrumented walkway with five embedded force plates (BP400600, AMTI, Watertown, MA; 9286AA, Kistler, Winterthur, Switzerland) was built to produce a repeatable step on a coronally uneven and unpredictable surface (details in Ref. [19]). Briefly, the middle force plate could be rigidly positioned either flush with the walkway or in a 15 deg inverted or 15 deg everted position. This angle could also be concealed (blinded) with a 0.5 mm opaque latex cover of negligible stiffness to minimize the participant's anticipatory adaptations prior to initial contact with the uneven step. A 15 deg angle was chosen because it is approximately half of the maximum range of coronal ankle motion [20–22], which minimized the possibility of injury. This isolated coronal plane disturbance simulated a singular step on an uneven surface such as walking on grass or rocks or stepping on the lateral edge of a sidewalk.

In-shoe plantar pressure was recorded at a sampling rate of 60 Hz, transmitted via Bluetooth and wirelessly synced with the motion capture system using the Pedar Insole System (99 sensors per insole, <2% error for loads between 500 and 1000 N [23]; Novel, Munich, Germany). Available in a variety of sizes, the insole pairs were fit to the participant's shoe size and placed on top of the existing insoles.

A 12-camera MX motion capture system (Vicon Motion Systems, Oxford, UK) recorded marker trajectories at 120 Hz and force plate data at 1200 Hz. A digital, fourth-order, low-pass Butterworth filter was applied with cutoff frequencies of 25 Hz (kinetics) and 6 Hz (kinematics). Filtered GRF data were exported to MATLAB (The MathWorks, Inc., Natick, MA), where they were combined with plantar pressure data according to the proportionality assumption [16] to produce individual foot segment GRFs and center of pressures (CoPs) and re-applied to the MSFM (shown in Fig. S1, which is available under the "Supplemental Materials" tab for this paper on the ASME Digital Collection).

2.3 Multisegment Foot Model and Shoe Modifications. The same investigator placed tracking markers directly to the skin of all participants after multiple holes were cut in standardized walking shoes (M577, New Balance, Boston, MA, sizes 5–12), exposing the foot's bony landmarks required for the MSFM (Fig. 1, [15,24]). A heel alignment device was also used according to Simon et al. to facilitate repeatable placement of the medial and lateral calcaneus markers [25]. To maintain the shoes' integrity, the navicular and cuboid static markers were placed on the leather upper of the shoe directly above each bony landmark (accurate to within 5 mm compared to skin mounted marker placement [26]). The on-shoe marker placement minimally affected joint kinetics because the thickness of the shoe contributed equally to the static marker positions, with their midpoint used to define the midtarsal joint (MTJ) center. An additional marker was also placed on the fifth metatarsal head (MT5) to define the width of the foot. The shank segment definition was similar to Bruening et al. [24]; however, the tracking markers were placed on bony landmarks (tibial tuberosity, fibular head, and lateral ankle malleolus) instead of a marker cluster. The plantar pressure insole positions were defined statically (Fig. 1) and tracked relative to the foot markers to establish local coordinates of the sensors relative to the lab's global coordinate system.

Fig. 1 Foot and sensor static marker placement with shoe cutouts to accommodate the in-shoe MSFM. The static sensor markers (red circles) were used to locate the position of the insoles relative to the location of the foot markers. All foot tracking markers were attached directly to the skin. The cuboid and navicular bony landmarks were palpated before subjects donned the shoes. Then markers (white circles) were attached to the shoe upper above the palpated location for the static trial only to define the MTJ center.

Each foot was modeled as three separate segments (hindfoot, forefoot, and hallux) according to Bruening et al. [15,24] and also combined into a single whole foot segment defined proximally at the ankle joint center (AJC) and distally at the metatarsophalangeal joint (MPJ). These segments were used to define four joints: whole foot relative to tibia (AJC_{WF}), hindfoot relative to tibia (AJC_{HF}), forefoot relative to hindfoot (MTJ), and hallux relative to forefoot (MPJ). Model details are shown in Figs. S2 and S5, which are available under the "Supplemental Materials" tab for this paper on the ASME Digital Collection. This model was chosen because of its demonstrated repeatable and reliable kinetic and kinematic results for the complete stance phase of gait [15,24] and because it could be adapted for shod walking. Other existing kinetic MSFMs were unable to capture early stance dynamics [17] or required too many segments to accommodate shod gait analysis [16]. An in-shoe MSFM was deemed most relevant for this study because individuals are typically shod during outdoor activities, where falls due to extrinsic factors such as uneven terrain are more common [1,2]. Furthermore, patients with lower limb pathologies often use footwear to reduce joint loading or accommodate orthoses/prostheses. Therefore, the knowledge acquired from shod gait on uneven terrain may be best suited as a comparative tool or to establish intervention design requirements. We tested the in-shoe kinetic foot model approach with a direct comparison to simultaneous measurements under subareas of the foot using adjacent force plates. The results of that comparison are shown in Fig. S3, which is available under the "Supplemental Materials" tab for this paper on the ASME Digital Collection.

2.4 Protocol. After completing instrumentation, participants walked at their self-selected speed across the walkway and stepped on the uneven surface with their dominant foot. Side dominance was determined by asking participants which foot they used to kick a ball [27]. Participants performed five repeated trials per condition (flush, inverted, and everted) with the center plate visible (unblinded). Before each unblinded condition, participants walked across the walkway several times to establish familiarity and proper foot positioning. Next, the opaque cover was placed over the center plate to blind participants to the disturbance condition, which was switched in a random order between each trial while participants waited in a separate room. This process was repeated approximately 15 times to achieve at least four repeated trials for each disturbance condition (flush, inverted, and everted). Only trials with a single foot contact were included in the analysis. Unblinded flush served as the baseline condition for undisturbed gait and the comparison for blinded inverted and blinded everted conditions.

2.5 Analysis Metrics. Spatiotemporal metrics included stance time and walking speed, which were calculated using the center-of-mass (CoM) velocity along the direction of progression. CoM velocity was calculated by taking the time derivative of the CoM position, which was calculated in Visual 3D (C-Motion, Germantown, MD) based on a 15-segment, modified Plug-In Gait (Vicon Motion Systems, Ltd., Oxford, UK) [28], whole-body model (details in Ref. [19]) using body segment masses and moments of inertia based on Dempster [29] and segment geometries. All joint angles and moments were also calculated in Visual 3D using a standard inverse dynamics approach [30,31]. All variables were time normalized to the gait cycle using force plate data to detect heel strike and toe off events. All kinetic metrics were normalized by the subject's body mass. Because both left and right foot dominant participants were tested, left foot data were negated to match the polarity of the right foot.

The ankle (AJC_{HF}, hindfoot–tibia = hindfoot relative to the tibia), midtarsal (MTJ, forefoot–hindfoot), metatarsophalangeal (MPJ, hallux-forefoot), and the whole foot ankle (AJC_{WF}) joint angles were calculated using an *XYZ* Euler angle sequence (positive *y*-axis was defined in the forward direction, positive *x*-axis was defined to the right, and positive *z*-axis was upwards, Fig. S5, which is available under the "Supplemental Materials" tab for this paper on the ASME Digital Collection), rotating the distal segment relative to the proximal segment. The static pose was used to define a neutral reference position of the foot whose angles were subtracted from all walking trials, similar to prior study (i.e., see Ref. [32]). Net internal joint moments were also calculated about each defined joint center for the distal relative to the proximal segment. For each trial, the coronal plane joint angles and moments were evaluated at peak loading during early stance and late stance, based on the first peak vertical GRF in the first half of stance phase and the second peak vertical GRF in the second half of stance phase, respectively (Fig. 2). We focused the analysis on coronal plane joint angles and moments because we anticipated that a step on a coronally uneven surface would elicit the largest response in this plane. However, sagittal and transverse plane angle and moment plots are also shown in Figs. S10 and S11, which are available under the "Supplemental Materials" tab for this paper on the ASME Digital Collection.

Total joint power was calculated as the dot product of the corresponding joint moment and joint angular velocity vectors using MATLAB software (The MathWorks, Inc., Natick, MA), similar to prior MSFM studies [15,16]. The three individual terms of the dot product were also illustrated in Fig. S12, which is available under the "Supplemental Materials" tab for this paper on the ASME Digital Collection, as representations of the three orthogonal axes (sagittal, coronal, and transverse). Total negative work, total positive work, and net work (total negative + total positive work) across stance phase were calculated for each joint using trapezoidal numerical time integration of the corresponding joint power. Total push-off work was also calculated as the time integral across the positive power burst in terminal stance (~70–100% stance) according to Winter [33]. The final metric we extracted was power at opposite heel contact (@OHC), because OHC corresponds to the end of the angular loading phase when the load is typically high [34] and may provide insight for emulating ankle function on coronally uneven terrain.

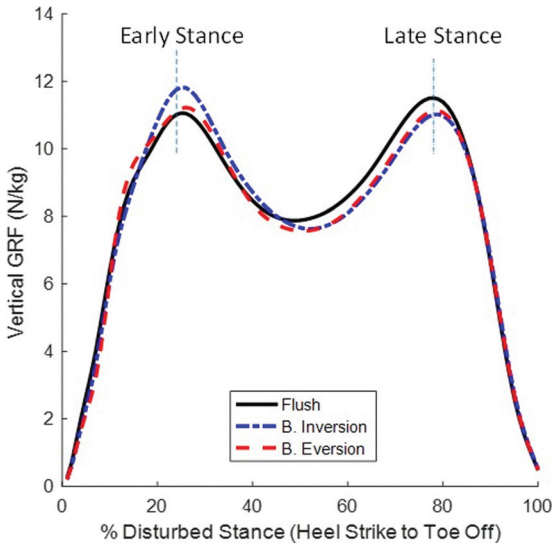

Fig. 2 Average vertical GRF normalized to body mass (N/kg) across the disturbed step stance phase for three surface conditions: flush, blinded (B.) inversion and B. eversion. The average timing of peak GRF in early stance and late stance, displayed with vertical dashed lines, were similar in timing across conditions. For each trial, the corresponding joint angles and moments at these peak loading events were also extracted (see Fig. 3).

2.6 Statistical Methods. Linear mixed-effects regression was used to detect differences in the biomechanical metrics (dependent variables) between surfaces (flush, blinded everted, and blinded inverted were the independent variables) for each joint separately (AJC_{WF}, AJC_{HF}, MTJ, and MPJ), with random effects for mean outcome and mean difference in outcome across surface by subject. An omnibus test for significance was generated using a likelihood ratio test with an alpha level of 0.05. Individual pairwise differences were assessed using simultaneous inference [35] and associated 95% confidence intervals (CIs). Analyses were carried out using R 3.3.1 (R Foundation for Statistical Computing, Vienna, Austria, 2016), the lme4 package [36] to carry out the linear regressions and the multcomp package [35] for simultaneous inference. Select average percent differences were also calculated as the average change divided by the largest mean value to facilitate comparisons across joints and metrics by emphasizing the relative size of the differences.

3 Results

Mean walking speed was similar (<5% average difference) across all surface conditions (Table 1). The inverted surface stance time was statistically less than the everted surface; however, this difference was relatively small (Δ0.02 s, 3%).

The largest changes in joint angles and moments occurred in the coronal plane, as expected (Fig. 3). AJC_{HF} conformed to the surface in early stance with increased eversion (Δ9.0 deg, 74%) and increased inversion (Δ10.7 deg, 143%) for the everted and inverted surfaces, respectively, compared to flush (Table 2; note:

Table 1 Mean (SE) spatio-temporal metrics for three surface conditions: flush, blinded (B.) eversion and B. inversion. An overall test for significance across surface (surface effect), mean pairwise differences (95% CI) and associated *P* values are also reported.

	Surface effect	Flush	B. Eversion	B. Inversion	B. Eversion—flush	B. Inversion—flush	B. Eversion—B. Inversion
Spatio-temporal variables	*P* value	Mean (SE)			Mean difference [95% CI], *P* value		
Walking speed (m/s)	0.18	1.213 (0.036)	1.238 (0.033)	1.250 (0.033)	0.025 [−0.021, 0.071], 0.40	0.037 [−0.012, 0.086], 0.18	−0.011 [−0.030, 0.007], 0.30
Stance time (s)	0.0098	0.700 (0.023)	0.694 (0.024)	0.675 (0.026)	−0.006 [−0.029, 0.017], 0.80	−0.025 [−0.052, 0.002], 0.73	0.019 [0.006, 0.031], 0.0014

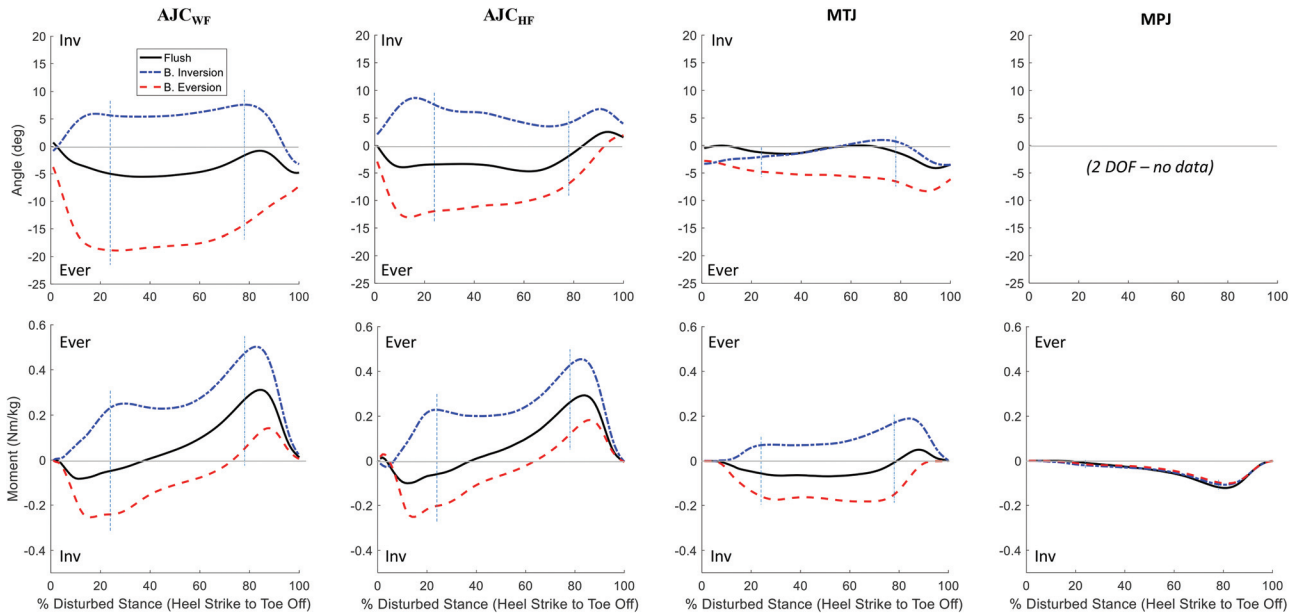

Fig. 3 Average coronal plane angles (deg, inversion+) and moments normalized by body mass (N·m/kg, eversion+) across the disturbed step stance phase (%) for three surface conditions: flush, blinded (B.) inversion and B. eversion and three joints: whole foot ankle (AJC_{WF}), hindfoot ankle (AJC_{HF}) and MTJ. The MPJ was modeled with two degrees-of-freedom (2DOF); therefore, only MPJ coronal moments were shown. Vertical dashed lines identify the average timing of peak vertical GRF in early stance and late stance, as shown in Fig. 2.

all reported subsequent changes are relative to the flush surface unless otherwise specified). Midtarsal only conformed to the everted surface in early stance (Δ3.3 deg, 72%). In late stance, AJC_{HF} remained conformed in the direction of the surfaces, albeit by smaller magnitudes (Δ5.3 deg eversion, 77%; Δ5.8 deg inversion, 138%) and MTJ further conformed in the direction of each surface compared to early stance (Δ5.4 deg eversion, 79%; Δ1.8 deg inversion, 138%). Finally, the total range of motion (RoM) for AJC_{HF} increased for the everted surface only (Δ6.7 deg, 43%), whereas MTJ RoM remained consistent across surfaces.

Joint moments were also affected by surface condition (Table 3), even at times when minimal angular changes were observed. In early stance, AJC_{HF} increased inversion moment (Δ0.173 N·m/kg, 74%) and increased eversion moment (Δ0.291 N·m/kg, 126%) for the everted and inverted surfaces, respectively. MTJ also demonstrated increased inversion moment on an everted surface (Δ0.091 N·m/kg, 60%) and increased eversion moment on an inverted surface (Δ0.127 N·m/kg, 191%), despite no change in MTJ angle for an inverted surface in early stance. This pattern was similar in late stance for both AJC_{HF} and MTJ. However, compared to early stance, the magnitudes decreased for AJC_{HF} on an everted (Δ0.135 N·m/kg, 52%) and inverted (Δ0.182 N·m/kg, 41%) surface, while they increased for MTJ on an everted (Δ0.147 N·m/kg, 100%) and inverted (Δ0.179 N·m/kg, 106%) surface. MPJ was less affected by changes in surface compared to the proximal foot joints, with a smaller magnitude increase in inversion moment on the inverted surface (Δ0.010 N·m/kg, 48%) in early stance and a smaller magnitude decrease in inversion moment on the everted surface (Δ0.023 N·m//kg, 19%) in late stance.

The effect of surface condition on total work varied by joint (Fig. 4 and Table 4). AJC_{HF} generated more positive work for an everted surface compared to inverted (Δ0.066 J/kg, 26%) or flush (Δ0.065 J/kg, 22%). AJC_{WF} presented a similar pattern with relatively smaller increases for an everted surface compared to inverted and flush (Δ0.035 and Δ0.042 J/kg, respectively, both 12%). In contrast, MTJ generated more positive work for an inverted compared to an everted (Δ0.025 J/kg, 33%) or flush (Δ0.027 J/kg, 36%) surface. MPJ positive work was equivalent across surfaces and an order of magnitude smaller than AJC_{HF} and MTJ.

AJC_{HF} negative work decreased for an everted (Δ0.032 J/kg, 27%) and inverted (Δ0.023 J/kg, 20%) surface. AJC_{WF} presented

Table 2 Mean (SE) coronal angle (deg) at corresponding peak loading events (early and late stance) and total RoM across the disturbed step stance phase (%) for three surface conditions: flush, blinded (B.) eversion and B. inversion and four joints: whole foot ankle (AJC_{WF}), hindfoot ankle (AJC_{HF}), midtarsal (MTJ), and metatarsophalangeal (MPJ). An overall test for significance across surface (surface effect), mean pairwise differences (95% CI) and associated *P* values are reported, with bold font emphasizing the significantly different mean surface value(s).

	Surface effect	Flush	B. Eversion	B. Inversion	B. Eversion—flush	B. Inversion—flush	B. Eversion—B. Inversion
Coronal angles (degrees)	*P* value	Mean (SE)			Mean difference [95% CI], *P* value		
Angle (Early stance)							
AJC_{WF}	<0.0001	**−5.0 (1.0)**	**−18.6 (1.1)**	**5.6 (0.9)**	−13.7 [−14.9, −12.5], <0.0001	10.6 [9.0, 12.3], <0.0001	−24.3 [−25.6, −23.1], <0.0001
AJC_{HF}	<0.0001	**−3.2 (1.2)**	**−12.2 (1.7)**	**7.5 (1.4)**	−9.0 [−11.7, −6.2], <0.0001	10.7 [7.8, 13.5], <0.0001	−19.6 [−21.7, −17.5], <0.0001
MTJ	0.0004	−1.3 (0.8)	**−4.6 (1.0)**	−2.2 (1.0)	−3.3 [−4.8, −1.9], <0.001	−0.9 [−2.9, 1.1], 0.52	−2.4 [−4.3, −0.6], 0.006
MPJ		(2 DOF model—no data)				(2 DOF model—no data)	
Angle (Late stance)							
AJC_{WF}	<0.0001	**−1.9 (1.1)**	**−14.3 (1.2)**	**7.5 (0.9)**	−12.4 [−13.3, −11.5], <0.0001	9.4 [8.1, 10.6], <0.0001	−21.7 [−23.3, −20.1], <0.0001
AJC_{HF}	<0.0001	**−1.6 (1.4)**	**−6.9 (1.5)**	**4.2 (1.7)**	−5.3 [−6.7, −3.8], <0.0001	5.8 [3.8, 7.9], <0.0001	−11.1 [−13.0, −9.3], <0.0001
MTJ	0.0004	**−1.3 (1.0)**	**−6.8 (1.4)**	**0.5 (1.0)**	−5.4 [−6.9, −4.0], <0.001	1.8 [0.3, 3.4], 0.018	−7.3 [−9.3, −5.3], <0.001
MPJ		(2 DOF model—no data)				(2 DOF Model—no data)	
Angle (RoM)							
AJC_{WF}	<0.0001	**8.4 (0.6)**	16.4 (1.1)	12.3 (1.1)	8.0 [5.2, 10.9], <0.001	3.9 [1.5, 6.4], <0.001	4.1 [−0.1, 8.2], 0.055
AJC_{HF}	<0.0001	8.9 (0.9)	**15.6 (1.0)**	8.8 (0.9)	6.7 [5.2, 8.3], <0.001	−0.1 [−2.7, 2.5], 0.99	6.8 [3.8, 9.9], <0.001
MTJ	0.2	5.2 (0.4)	6.6 (0.9)	6.1 (0.5)	1.4 [−0.6, 3.4], 0.25	0.9 [−0.7, 2.6], 0.39	0.4 [−1.8, 2.7], 0.89
MPJ		(2 DOF model—no data)				(2 DOF Model—no data)	

Table 3 Mean (SE) coronal moments normalized to body mass (N·m/kg) at corresponding peak loading events (early and late stance) for three surface conditions: flush, blinded (B.) eversion, and B. inversion and four joints: whole foot ankle (AJC_{WF}), hindfoot ankle (AJC_{HF}), midtarsal (MTJ), and metatarsophalangeal (MPJ). An overall test for significance across surface (surface effect), mean pairwise differences (95% CI) and associated *P* values are reported, with bold font emphasizing the significantly different mean surface value(s).

	Surface effect	Flush	B. Eversion	B. Inversion	B. Eversion—flush	B. Inversion—flush	B. Eversion—B. Inversion
Coronal moments (N·m/kg)	*P* value	Mean (SE)			Mean difference [95% CI], *P* value		
Moment (early stance)							
AJC_{WF}	<0.0001	**−0.046 (0.011)**	**−0.258 (0.016)**	**0.241 (0.013)**	−0.212 [0.184, 0.241], <0.0001	0.287 [−0.313, −0.260], <0.0001	−0.499 [0.455, 0.543], <0.0001
AJC_{HF}	<0.0001	**−0.061 (0.010)**	**−0.230 (0.014)**	**0.230 (0.022)**	−0.173 [0.140, 0.205], <0.0001	0.291 [−0.339, −0.243], <0.0001	−0.464 [0.405, 0.522], <0.0001
MTJ	<0.0001	**−0.059 (0.009)**	**−0.151 (0.012)**	**0.068 (0.011)**	−0.091 [0.066, 0.116], <0.0001	0.127 [−0.143, −0.111], <0.0001	−0.218 [0.185, 0.251], <0.0001
MPJ	0.022	−0.010 (0.003)	−0.013 (0.004)	**−0.021 (0.004)**	−0.002 [−0.004, 0.008], 0.67	−0.010 [0.002, 0.018], 0.010	0.008 [−0.014, −0.002], 0.0068
Moment (late stance)							
AJC_{WF}	<0.0001	**0.259 (0.027)**	**0.052 (0.029)**	**0.482 (0.024)**	0.208 [0.172, 0.243], <0.0001	0.223 [−0.243, −0.202], <0.0001	−0.431 [0.401, 0.460], <0.0001
AJC_{HF}	<0.0001	**0.254 (0.023)**	**0.119 (0.026)**	**0.436 (0.027)**	0.135 [0.100, 0.170], <0.0001	0.182 [−0.208, −0.160], <0.0001	−0.317 [0.286, 0.348], <0.0001
MTJ	<0.0001	**−0.007 (0.018)**	**−0.154 (0.013)**	**0.172 (0.020)**	−0.147 [0.111, 0.184], <0.0001	0.179 [−0.199, −0.158], <0.0001	−0.326 [0.289, 0.363], <0.0001
MPJ	0.042	−0.119 (0.012)	**−0.096 (0.012)**	−0.105 (0.011)	0.023 [−0.044, −0.001], 0.042	0.014 [−0.029, 0.002], 0.095	0.009 [−0.032, 0.015], 0.65

a similar pattern as AJC_{HF}; however, the differences did not reach statistical significance. In contrast, MTJ negative work increased for an everted compared to a flush (Δ0.026 J/kg, 22%) or an inverted (Δ0.041 J/kg, 35%) surface. Finally, MPJ negative work increased for an inverted compared to an everted (Δ0.013 J/kg, 17%) and flush (Δ0.009 J/kg, 12%) surface; however, the MPJ negative work contributions were at least half the magnitude compared to the proximal foot joints.

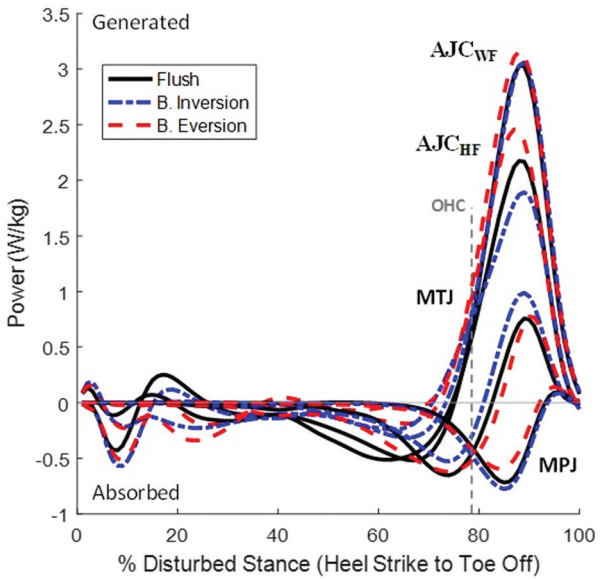

Fig. 4 Average total power normalized by body mass (W/kg, generated+) across the disturbed step stance phase (%) for three surface conditions: flush, blinded (B.) inversion and B. eversion and four joints: whole foot ankle (AJC$_{WF}$), hindfoot ankle (AJC$_{HF}$), midtarsal (MTJ), and metatarsophalangeal (MPJ). A vertical dashed line portrays the average percent stance time of the OHC (OHC 79 ± 2%).

AJC$_{HF}$ net total work was positive for all surfaces and increased for an everted compared to a flush (Δ0.097 J/kg, 51%) and inverted (Δ0.075 J/kg, 40%) surface. Again, AJC$_{WF}$ presented larger total work magnitudes and a similar albeit smaller surface effect as AJC$_{HF}$, with smaller increases for an everted compared to a flush (Δ0.060 J/kg, 25%) and an inverted (Δ0.040 J/kg, 17%) surface. In contrast, MTJ net total work was negative for all surfaces; the everted surface was more negative (Δ0.024 J/kg, 36%), while the inverted surface was less negative and close to zero (Δ0.041 J/kg, 95%).

The surface effect on push-off work in terminal stance was similar to the results for positive total work, which was an expected finding because the majority of work (96.5 ± 1.5%) was performed during this phase (Table 5). Power @OHC, which occurred at 79 ± 2% stance, was positive for AJC$_{HF}$ and increased for an everted (Δ0.607 W/kg, 57%) and inverted (Δ0.379 W/kg, 38%) surface, similar to AJC$_{WF}$. In contrast, power @OHC was negative for MTJ and MPJ across surfaces, with MTJ less negative for an inverted surface (Δ0.344 W/kg, 67%) and MPJ more negative for an inverted surface (Δ0.161 W/kg, 30%).

The sum of positive total work for all MSFM joints (AJC$_{HF}$ + MTJ + MPJ, Table 4) increased for an everted (Δ0.069 J/kg, 21%) and inverted (Δ0.027 J/kg, 10%) surface. The sum of negative total work only decreased for the inverted surface (Δ0.028 J/kg, 11%). However, when combined, the sum of net total work across all joints increased for an everted (Δ0.078 J/kg, 127%) and inverted (Δ0.055 J/kg, 125%) surface resulting in positive net total work for an uneven surface versus negative net total work for the flush surface.

4 Discussion

The complexities of the foot and ankle joints are frequently overlooked by studies that model the ankle as a simple hinge joint, disregarding its ability to conform to the surface, and actively resist and distribute loads [37]. While the simplified model may be appropriate for studying ambulation on flat surfaces, this approach is likely insufficient for measuring the foot's ability to adapt to coronally uneven terrain. Furthermore, due to the complexities of modeling a multi-articulating foot, few studies have examined the joint kinetics associated with this common and more complex task. Therefore, the purpose of this study was to identify the foot biomechanical adaptations required for a step on an unpredictable coronally uneven surface. We found that the effect of surface was largest for AJC$_{HF}$ coronal plane biomechanics in early stance; however, distinct differences were also observed for the MTJ (especially in late stance) and MPJ. Coronal plane differences for MPJ only occurred on the inverted surface and were relatively small compared to the proximal joints; therefore, the succeeding discussion will focus on the larger differences found at AJC$_{HF}$ and MTJ.

4.1 Kinematics. The MSFM angles on a flush surface were similar in shape and RoM to those reported in prior study using the same model [24] and other similar three-segment foot models [16,17,38]. The partial decoupling of the hindfoot and forefoot segments ("elica podalica" [39]) is accentuated during a step on an uneven surface. In early stance, AJC$_{HF}$ conformed most (∼10 deg) in the same direction as the uneven surface with increased inversion on the inverted surface and increased eversion on the everted surface, which was consistent with prior study [20]. MTJ further everted (∼3 deg) on the everted surface only in early stance. However, as the load shifted onto the forefoot in late stance, MTJ further conformed to the everted surface (∼5 deg) and also conformed to the inverted surface (∼2 deg). In late stance, AJC$_{HF}$ still conformed in the direction of the uneven surface, but only about half as much compared to early stance (∼5 deg). This sequential partial decoupling between the two joints is consistent with prior literature [11,12], which serves to maximize plantar surface contact and maintain a stable base of support. Despite a similar interpretation, Damavandi et al. [11] reported coronal plane hindfoot angles at heel strike that were opposite to the angle of the surface (i.e., everted surface was inverted and inverted surface was everted until 10% stance), which may be related to the anticipatory response of increased peroneal [7] and decreased tibialis anterior [6] muscle activity. In contrast, the direction (inverted/everted) of the surface was unknown to our participants, thus eliminating direction specific anticipatory behavior. Damavandi et al. [11] also reported opposite coronal versus surface angles for the forefoot in early stance; however, in late stance when forefoot angle differences were largest and anticipation effects reduced, the angles were consistent with the surface angle and similar to our findings. However, they also reported AJC$_{HF}$ returned to an everted position for all surfaces in late stance, which contrasted our findings of continued conformation in the direction of the uneven surface. Methodological differences including walking barefoot on a known 10 deg cross-slope versus this study's shod step on a concealed 15 deg coronally angled surface likely contributed to these differences.

4.2 Kinetics. Joint moments during a step on a coronally uneven surface provide comprehensive force production estimates that correlate well with the onset of muscular activity [8]. The MSFM coronal moments we found during shod flush walking were similar in shape and magnitude to prior study of barefoot walking [15]. For an inverted surface in early stance, we found AJC$_{HF}$ and MTJ increased eversion moment (126% and 191%, respectively), which corresponds to a medial shift in CoP [40] and recruitment of late-latency peroneals and gastrocnemius muscle activations for stretch resistance, balance control and load reduction [6,8] as the foot conforms to the inverted surface. In late stance, eversion moment approximately doubled for both joints and coupled with smaller angular conformations, which implied increased coronal plane joint stiffness facilitated push-off. Therefore, the foot's complex structure provided coronal plane flexibility to conform to the surface and absorb shock during loading with stiffening in later stance to facilitate propulsion [39,41].

For an everted surface in early stance, the similar increased inversion moments for AJC$_{HF}$ and MTJ (74% and 60%,

Table 4 Mean (SE) total positive, negative and net joint work normalized to body mass (J/kg) across the disturbed step stance phase (%) for three surface conditions: flush, blinded (B.) eversion and B. inversion and four joints: whole foot ankle (AJC_{WF}), hindfoot ankle (AJC_{HF}), midtarsal (MTJ), and metatarsophalangeal (MPJ); the sum of all MSFM joints (AJC_{HF} + MTJ + MPJ) was also included. An overall test for significance across surface (surface effect), mean pairwise differences (95% CI) and associated *P* values are reported, with bold font emphasizing the significantly different mean surface value(s).

	Surface effect	Flush	B. Eversion	B. Inversion	B. Eversion—flush	B. Inversion—flush	B. Eversion—B. Inversion
Total work (J/kg)	*P* value	Mean (SE)			Mean difference [95% CI], *P* value		
Positive work							
AJC_{WF}	0.0026	0.295 (0.018)	**0.337 (0.022)**	0.302 (0.018)	0.042 [0.017, 0.067], 0.0003	0.007 [−0.016, 0.029], 0.78	0.035 [0.013, 0.056], 0.0003
AJC_{HF}	0.0003	0.209 (0.013)	**0.273 (0.020)**	0.208 (0.016)	0.065 [0.039, 0.090], <0.0001	0.002 [−0.020, 0.017], 0.98	0.066 [0.039, 0.095], <0.0001
MTJ	0.0009	0.048 (0.009)	0.051 (0.007)	**0.075 (0.010)**	0.003 [−0.009, 0.014], 0.85	0.027 [0.014, 0.040], <0.0001	−0.025 [−0.037, −0.012], <0.0001
MPJ	0.041	0.005 (0.001)	0.006 (0.001)	0.005 (0.001)	0.001 [0.000, 0.003], 0.055	0.001 [−0.001, 0.002], 0.42	0.001 [−0.002, 0.003], 0.59
AJC_{HF} + MTJ + MPJ	<0.0001	**0.262 (0.020)**	**0.331 (0.025)**	**0.289 (0.023)**	0.069 [0.046, 0.091], <0.001	0.027 [0.002, 0.051], 0.028	0.042 [0.011, 0.073], 0.0036
Negative work							
AJC_{WF}	0.13	−0.113 (0.012)	−0.094 (0.011)	−0.098 (0.010)	0.018 [−0.005, 0.042], 0.16	0.014 [−0.003, 0.031], 0.13	0.004 [−0.017, 0.025], 0.88
AJC_{HF}	0.011	**−0.117 (0.013)**	−0.085 (0.010)	−0.094 (0.011)	0.032 [0.006, 0.057], 0.01	0.023 [0.004, 0.042], 0.014	0.009 [−0.019, 0.037], 0.74
MTJ	0.0062	−0.092 (0.009)	**−0.118 (0.010)**	−0.077 (0.010)	−0.026 [−0.043, −0.009], <0.001	0.014 [−0.003, 0.031], 0.12	−0.041 [−0.065, −0.016], <0.001
MPJ	0.0059	−0.068 (0.004)	−0.064 (0.005)	**−0.077 (0.004)**	0.004 [−0.004, 0.011], 0.50	−0.009 [−0.017, −0.001], 0.020	0.013 [0.005, 0.020], <0.001
AJC_{HF} + MTJ + MPJ	0.001	−0.277 (0.012)	−0.269 (0.012)	**−0.249 (0.011)**	0.009 [−0.010, 0.028], 0.47	0.028 [0.013, 0.043], <0.001	−0.018 [−0.037, 0.000], 0.053
Net work							
AJC_{WF}	0.0026	0.183 (0.021)	**0.243 (0.022)**	0.203 (0.019)	0.060 [0.027, 0.093], <0.001	0.020 [−0.014, 0.055], 0.35	0.040 [0.009 0.070], 0.0063
AJC_{HF}	0.0001	0.092 (0.021)	**0.189 (0.024)**	0.113 (0.022)	0.097 [0.062, 0.131], <0.001	0.021 [−0.005, 0.048], 0.13	0.075 [0.034, 0.117], <0.001
MTJ	<0.0001	**−0.043 (0.013)**	**−0.067 (0.012)**	**−0.002 (0.015)**	−0.024 [−0.040, −0.008], 0.0013	0.041 [0.026, 0.057], <0.001	−0.065 [−0.088, −0.043], <0.001
MPJ	0.0028	−0.063 (0.004)	−0.058 (0.005)	**−0.072 (0.004)**	0.005 [−0.002, 0.012], 0.24	−0.009 [−0.016, −0.001], 0.02	0.014 [0.006, 0.021], <0.001
AJC_{HF} + MTJ + MPJ	<0.0001	**−0.015 (0.021)**	0.063 (0.023)	0.040 (0.025)	0.078 [0.055, 0.101], <0.001	0.055 [0.032, 0.077], <0.001	0.023 [0.003, 0.049], 0.092

respectively) corresponded to a lateral shift in CoP [40], which was likely controlled by the ankle invertors (primarily tibialis posterior) providing dynamic support and shock absorption [41]. However, in late stance when AJC_{HF} switched to an eversion moment, MTJ remained with an inversion moment similar in magnitude to the moment in early stance, likely because it remained conformed to the everted surface and only approached zero in terminal stance. These differing joint moments in late stance in conjunction with sequential kinematic decoupling and the previously reported dissociation of intrinsic foot muscle activation during sideways gait [42], provide further support of the foot's distinct mechanical role to be compliant and actively respond to perturbations [37].

Multisegment foot model joint powers provide insight into energy transfer across joints by providing estimates of the angle-moment relationships across the gait cycle. Across all joints, scalar joint power during shod flush ambulation was similar in shape and magnitude to prior studies [15–17], with average peak differences ($\leq$0.5 W/kg) likely attributed to differences in walking speed and barefoot versus shod ambulation (Fig. 4). We found significant AJC_{HF} and MTJ work generated at push-off while MPJ almost exclusively absorbed work (Table 5). The AJC_{WF}'s over-estimated push-off work across surfaces ($\sim$27%) compared to AJC_{HF} was likely because AJC_{WF} did not factor in MPJ absorption, consistent with the aforementioned studies.

AJC_{HF} and AJC_{WF} power and work were similarly affected by surface, albeit smaller differences between surfaces were found for AJC_{WF}. For an everted surface, AJC_{HF} generated 23% more push-off work compared to flush, whereas for an inverted surface, MTJ generated 34% more push-off work, implying differing joint strategies may exist for propulsion from an everted versus inverted surface. Reduced work absorbed coupled with increased work generated, led to increased net total work for AJC_{HF} on an everted surface (51%), which implies an active element with varying outputs dependent on surface may be required to mimic AJC_{HF} function. In contrast, increased work absorbed for MTJ on an everted surface resulted in increased *negative* net total work (36%), whereas increased work generated on an inverted surface resulted in reduced *negative* net total work (95%) that was close to zero (neutral). Despite these differing surface effects on MTJ work, the net total work remained negative across conditions, implying that a passive device with different stiffness profiles could replicate its function on a coronally uneven surface.

Power @OHC that corresponds to the high loads that typically occur at the end of the angular loading phase, may provide further insight for the design of mechanical devices that emulate ankle function [34]. AJC_{HF} power @OHC was positive across all conditions, with larger values for inverted and everted surfaces, implying a more powerful active element may be required for uneven terrain. Our flush results differ from Hansen et al. [34],

Table 5 Mean (SE) joint work at push-off (J/kg) and joint power (W/kg) @OHC normalized to body mass for three surface conditions: flush, blinded (B.) eversion and B. inversion and four joints: whole foot ankle (AJC_{WF}), hindfoot ankle (AJC_{HF}), midtarsal (MTJ), and metatarsophalangeal (MPJ). An overall test for significance across surface (surface effect), mean pairwise differences (95% CI) and associated *P* values are reported, with bold font emphasizing the significantly different mean surface value(s).

	Surface effect	Flush	B. Eversion	B. Inversion	B. Eversion—flush	B. Inversion—flush	B. Eversion—B. Inversion
Work (J/kg) and power (W/kg)	*P* value	Mean (SE)			Mean difference [95% CI], *P* value		
Push-off work							
AJC_{WF}	0.0007	0.277 (0.016)	**0.329 (0.021)**	0.287 (0.016)	0.052 [0.028, 0.075], <0.0001	0.010 [−0.012, 0.032], 0.53	0.041 [0.017, 0.066], 0.0002
AJC_{HF}	0.0011	0.201 (0.013)	**0.260 (0.022)**	0.200 (0.016)	0.059 [0.030, 0.088], <0.0001	0.004 [−0.026, 0.017], 0.88	0.063 [0.032, 0.094], <0.0001
MTJ	0.0033	0.046 (0.009)	0.049 (0.007)	**0.070 (0.011)**	0.003 [−0.008, 0.014], 0.77	0.024 [0.011, 0.036], 0.001	−0.021 [−0.035, −0.006], 0.004
MPJ	0.0066	−0.067 (0.003)	−0.063 (0.005)	**−0.076 (0.004)**	0.004 [−0.004, 0.011], 0.51	−0.009 [−0.017, −0.001], 0.027	0.013 [0.005, 0.020], <0.001
Power @OHC							
AJC_{WF}	0.0077	**0.618 (0.163)**	**1.329 (0.268)**	**1.041 (0.208)**	0.712 [0.283, 1.140], <0.001	0.423 [0.077, 0.770], 0.012	0.288 [0.005, 0.572], 0.045
AJC_{HF}	0.0021	**0.465 (0.178)**	1.072 (0.238)	0.844 (0.171)	0.607 [0.286, 0.927], <0.001	0.379 [0.040, 0.718], 0.025	0.228 [−0.187, 0.643], 0.40
MTJ	0.063	−0.510 (0.099)	−0.404 (0.154)	**−0.166 (0.188)**	0.106 [−0.161, 0.373], 0.62	0.344 [0.026, 0.662], 0.03	−0.237 [−0.526, 0.050], 0.13
MPJ	0.048	−0.379 (0.053)	−0.457 (0.057)	**−0.540 (0.072)**	−0.078 [−0.199, 0.043], 0.28	−0.161 [−0.307, −0.016], 0.025	0.083 [−0.005, 0.171], 0.068

who predicted slightly negative power @OHC (∼ −0.25 W/kg, from Fig. 7 in [34]) for participants walking on a flat surface at a comparable walking speed (∼1.2 m/s). Tracking the foot with markers placed directly on the skin (this study) versus shod marker placement may explain these differences. In contrast, MTJ and MPJ powers @OHC were negative across all surfaces, suggesting a passive device could accommodate these joints on both flush and uneven terrain. However, the inverted surface elicited differing effects, reducing MTJ (67%) while increasing MPJ (30%) negative power @OHC, suggesting that MPJ may have compensated for reduced MTJ absorption on an inverted surface.

The sum of all MSFM work ($AJC_{HF} + MTJ + MPJ$) serves as a proxy of total work performed at the foot-ankle complex on a coronally uneven surface. The positive work sum increased for the inverted surface (10%) and further increased for the everted surface (21%), while the negative work sum decreased for just the inverted surface (11%). The resulting net work performed increased for the everted (127%) and inverted (125%) surfaces, resulting in positive net work performed for both uneven conditions. This increased energy generation is consistent with the 28% increased metabolic cost that has been reported for walking on uneven terrain [43]. In contrast, the flush surface elicited negative net work, which has been previously observed for level ground walking [44]; however, our flush results were approximately half the magnitude compared to prior study (−0.015 J/kg versus −0.038 J/kg), which may be attributed to our model accounting for the energy transfer at MTJ and MPJ joints. Additionally, our model did not account for translational powers to remain consistent with prior MSFM literature, which reported high repeatability and reliability for this model [15,24]. Therefore, our power estimates did not account for the effects of soft-tissue and shoe deformations, which may have also contributed to the smaller negative net work magnitudes compared to prior study [44]. Using a repeatable MSFM with joint centers based on bony landmarks and standardized shoes likely mitigated these confounding effects and reduced between subject and condition variability.

Additional limitations of this study should be considered when interpreting the findings. Our unique experimental design provided insight into how the healthy foot-ankle complex accommodates an uneven surface through a controlled and repeatable paradigm but may not be generalizable for ambulating on all types of uneven terrain, across all shoe types or for patients with pathologies, especially those with neurological deficits. A small step down (∼2.7 cm) was also required to obscure the uneven surfaces and may have contributed to some of the observed differences. However, a study of a larger, 10 cm step down reported increased negative work at the AJC_{WF} for an unexpected versus expected step down [45], with both conditions exhibiting increased negative work compared to the AJC_{HF} negative work we observed on flush and uneven surfaces. This opposite effect for a more than three-fold larger step down may imply that the 15 deg surface and not the relatively small step down contributed to the decreased negative work we observed. However, further study that isolates the smaller step-down effect may be warranted.

5 Conclusions

A kinetic MSFM measured distinct foot joint biomechanical adaptations to a coronally uneven surface. The conventional AJC_{WF} model over-estimated ankle push-off work and minimized the foot-ankle complex adaptations on an uneven surface. The increased AJC_{HF} positive power @OHC on both uneven surfaces contrasted the negative values measured for MTJ and MPJ across surfaces. The clinical application of this finding implies that a more powerful active element may be required to accommodate uneven terrain at the ankle, while a passive element could emulate distal foot joint mechanics on a variety of terrains. Although smaller in magnitude compared to AJC_{HF}, MTJ conformed to the surface and accommodated the altered loads to maintain balance and facilitate propulsion, especially on an inverted surface. When these specific joint adaptations are combined across the foot-ankle complex, net work performed switched from a negative value (energy absorption) on a flush surface to larger positive values (energy generation) on both uneven surfaces. This increased foot-ankle energy generation, consistent with the increased metabolic cost reported in prior study, indicates significant contributions from both the ankle and foot joints are required for optimal performance on uneven terrain.

Acknowledgment

We would like to thank Janice Pecoraro, R. N., Jane Shofer, M. S., and Krista Cyr, M. S. for their contributions to the manuscript. The contents do not represent the views of the U.S. Department of Veterans Affairs or the United States Government.

Funding Data

- U.S. Department of Veterans Affairs, Rehabilitation Research and Development Service (Grant Nos. A9243C, A9248-S, and I01 RX001840).

Nomenclature

AJC_{HF} = ankle joint center—hindfoot
AJC_{WF} = ankle joint center—whole foot
B. Ever = blinded eversion
B. Inv = blinded inversion
CI = confidence interval
CoM = center of mass
CoP = center of pressure
Dorsi = dorsiflexion
Ext = external rotation
GRF = ground reaction force
Int = internal rotation
MPJ = metatarsophalangeal joint
MSFM = multisegment foot model
MTJ = midtarsal joint
MT1 = first metatarsal head
MT5 = fifth metatarsal head
Plantar = plantarflexion
RoM = range of motion
SE = standard error
@OHC = at opposite heel strike

References

[1] Li, W., Keegan, T. H. M., Sternfeld, B., Sidney, S., Quesenberry, C. P., Jr., and Kelsey, J. L., 2006, "Outdoor Falls Among Middle-Aged and Older Adults: A Neglected Public Health Problem," Am. J. Public Health, **96**(7), pp. 1192–1200.
[2] Niino, N., Tsuzuku, S., Ando, F., and Shimokata, H., 2000, "Frequencies and Circumstances of Falls in the National Institute for Longevity Sciences, Longitudinal Study of Aging (NILS-LSA)," J. Epidemiol., **10**(Suppl. 1), pp. S90–S94.
[3] Kelsey, J. L., Procter-Gray, E., Hannan, M. T., and Li, W., 2012, "Heterogeneity of Falls Among Older Adults: Implications for Public Health Prevention," Am. J. Public Health, **102**(11), pp. 2149–2156.
[4] Marigold, D. S., and Patla, A. E., 2008, "Age-Related Changes in Gait for Multi-Surface Terrain," Gait Posture, **27**(4), pp. 689–696.
[5] Keegan, T. H., Kelsey, J. L., King, A. C., Quesenberry, C. P., Jr., and Sidney, S., 2004, "Characteristics of Fallers Who Fracture at the Foot, Distal Forearm, Proximal Humerus, Pelvis, and Shaft of the Tibia/Fibula Compared With Fallers Who Do Not Fracture," Am. J. Epidemiol., **159**(2), pp. 192–203.
[6] Nieuwenhuijzen, P. H., and Duysens, J., 2007, "Proactive and Reactive Mechanisms Play a Role in Stepping on Inverting Surfaces During Gait," J. Neurophysiol., **98**(4), pp. 2266–2273.
[7] Forestier, N., and Toschi, P., 2005, "The Effects of an Ankle Destabilization Device on Muscular Activity While Walking," Int. J. Sports Med., **26**(6), pp. 464–470.
[8] Konradsen, L., Peura, G., Beynnon, B., and Renstrom, P., 2005, "Ankle Eversion Torque Response to Sudden Ankle Inversion Torque Response in Unbraced, Braced, and Pre-Activated Situations," J. Orthop. Res., **23**(2), pp. 315–321.
[9] Damavandi, M., Dixon, P. C., and Pearsall, D. J., 2012, "Ground Reaction Force Adaptations During Cross-Slope Walking and Running," Hum. Mov. Sci., **31**(1), pp. 182–189.
[10] Dixon, P. C., and Pearsall, D. J., 2010, "Gait Dynamics on a Cross-Slope Walking Surface," J. Appl. Biomech., **26**(1), pp. 17–25.
[11] Damavandi, M., Dixon, P. C., and Pearsall, D. J., 2010, "Kinematic Adaptations of the Hindfoot, Forefoot, and Hallux During Cross-Slope Walking," Gait Posture, **32**(3), pp. 411–415.
[12] Urry, S. R., 2002, "Redistribution of Foot Pressure in Healthy Adults During Sideslope Walking," Foot Ankle Int., **23**(12), pp. 1112–1118.
[13] Elftman, H., 1960, "The Transverse Tarsal Joint and Its Control," Clin. Orthop., **16**, pp. 41–46.
[14] Rolian, C., Lieberman, D. E., and Hallgrimsson, B., 2010, "The Coevolution of Human Hands and Feet," Evolution, **64**(6), pp. 1558–1568.
[15] Bruening, D. A., Cooney, K. M., and Buczek, F. L., 2012, "Analysis of a Kinetic Multi-Segment Foot Model—Part II: Kinetics and Clinical Implications," Gait Posture, **35**(4), pp. 535–540.
[16] MacWilliams, B. A., Cowley, M., and Nicholson, D. E., 2003, "Foot Kinematics and Kinetics During Adolescent Gait," Gait Posture, **17**(3), pp. 214–224.
[17] Dixon, P. C., Bohm, H., and Doderlein, L., 2012, "Ankle and Midfoot Kinetics During Normal Gait: A Multi-Segment Approach," J. Biomech., **45**(6), pp. 1011–1016.
[18] Bruening, D. A., Cooney, K. M., Buczek, F. L., and Richards, J. G., 2010, "Measured and Estimated Ground Reaction Forces for Multi-Segment Foot Models," J. Biomech., **43**(16), pp. 3222–3226.
[19] Yeates, K. H., Segal, A. D., Neptune, R. R., and Klute, G. K., 2016, "Balance and Recovery on Coronally-Uneven and Unpredictable Terrain," J. Biomech., **49**(13), pp. 2734–2740.
[20] Kim, H., and Ashton-Miller, J. A., 2012, "A Shoe Sole-Based Apparatus and Method for Randomly Perturbing the Stance Phase of Gait: Test-Retest Reliability in Young Adults," J. Biomech., **45**(10), pp. 1850–1853.
[21] Ottaviani, R. A., Ashton-Miller, J. A., Kothari, S. U., and Wojtys, E. M., 1995, "Basketball Shoe Height and the Maximal Muscular Resistance to Applied Ankle Inversion and Eversion Moments," Am. J. Sports Med., **23**(4), pp. 418–423.
[22] Ashton-Miller, J. A., Ottaviani, R. A., Hutchinson, C., and Wojtys, E. M., 1996, "What Best Protects the Inverted Weightbearing Ankle Against Further Inversion? Evertor Muscle Strength Compares Favorably With Shoe Height, Athletic Tape, and Three Orthoses," Am. J. Sports Med., **24**(6), pp. 800–809.
[23] Hurkmans, H. L., Bussmann, J. B., Benda, E., Verhaar, J. A., and Stam, H. J., 2006, "Accuracy and Repeatability of the Pedar Mobile System in Long-Term Vertical Force Measurements," Gait Posture, **23**(1), pp. 118–125.
[24] Bruening, D. A., Cooney, K. M., and Buczek, F. L., 2012, "Analysis of a Kinetic Multi-Segment Foot Model—Part I: Model Repeatability and Kinematic Validity," Gait Posture, **35**(4), pp. 529–534.
[25] Simon, J., Doederlein, L., McIntosh, A. S., Metaxiotis, D., Bock, H. G., and Wolf, S. I., 2006, "The Heidelberg Foot Measurement Method: Development, Description and Assessment," Gait Posture, **23**(4), pp. 411–424.
[26] Bishop, C., Thewlis, D., Uden, H., Ogilvie, D., and Paul, D., 2011, "A Radiological Method to Determine the Accuracy of Motion Capture Marker Placement on Palpable Anatomical Landmarks Through a Shoe," Footwear Sci., **3**(3), pp. 169–177.
[27] Sadeghi, H., Allard, P., Prince, F., and Labelle, H., 2000, "Symmetry and Limb Dominance in Able-Bodied Gait: A Review," Gait Posture, **12**(1), pp. 34–45.
[28] Ferrari, A., Benedetti, M. G., Pavan, E., Frigo, C., Bettinelli, D., Rabuffetti, M., Crenna, P., and Leardini, A., 2008, "Quantitative Comparison of Five Current Protocols in Gait Analysis," Gait Posture, **28**(2), pp. 207–216.
[29] Dempster, W. J., 1955, "Space Requirements for the Seated Operator," Wright Patterson Air Force Base, Dayton, OH, Technical Report No. WADC-TR-55-159.
[30] Winter, D. A., Patla, A. E., Frank, J. S., and Walt, S. E., 1990, "Biomechanical Walking Pattern Changes in the Fit and Healthy Elderly," Phys. Ther., **70**(6), pp. 340–347.
[31] Winter, D. A., 1991, "Changes in Gait With Aging," Can. J. Sport Sci., **16**(3), pp. 165–167.
[32] Deschamps, K., Staes, F., Roosen, P., Nobels, F., Desloovere, K., Bruyninckx, H., and Matricali, G. A., 2011, "Body of Evidence Supporting the Clinical Use of 3D Multisegment Foot Models: A Systematic Review," Gait Posture, **33**(3), pp. 338–349.
[33] Winter, D. A., 1983, "Energy Generation and Absorption at the Ankle and Knee During Fast, Natural, and Slow Cadences," Clin. Orthop. Relat. Res., (175), pp. 147–154.
[34] Hansen, A. H., Childress, D. S., Miff, S. C., Gard, S. A., and Mesplay, K. P., 2004, "The Human Ankle During Walking: Implications for Design of Biomimetic Ankle Prostheses," J. Biomech., **37**(10), pp. 1467–1474.
[35] Hothorn, T., Bretz, F., and Westfall, P., 2008, "Simultaneous Inference in General Parametric Models," Biom. J., **50**(3), pp. 346–363.
[36] Bates, D., Maechler, M., Bolker, B., and Walker, S., 2015, "Fitting Linear Mixed-Effects Models Using lme4," J. Stat. Software, **67**(1), pp. 1–48.
[37] Wright, W. G., Ivanenko, Y. P., and Gurfinkel, V. S., 2012, "Foot Anatomy Specialization for Postural Sensation and Control," J. Neurophysiol., **107**(5), pp. 1513–1521.
[38] Carson, M. C., Harrington, M. E., Thompson, N., O'Connor, J. J., and Theologis, T. N., 2001, "Kinematic Analysis of a Multi-Segment Foot Model for Research and Clinical Applications: A Repeatability Analysis," J. Biomech., **34**(10), pp. 1299–1307.
[39] Leardini, A., O'Connor, J. J., and Giannini, S., 2014, "Biomechanics of the Natural, Arthritic, and Replaced Human Ankle Joint," J. Foot Ankle Res., **7**(1), p. 8.
[40] Hof, A. L., van Bockel, R. M., Schoppen, T., and Postema, K., 2007, "Control of Lateral Balance in Walking. Experimental Findings in Normal Subjects and Above-Knee Amputees," Gait Posture, **25**(2), pp. 250–258.
[41] Perry, J., ed., 1992, *Gait Analysis: Normal and Pathological Function*, Slack Inc., Thorofare, NJ.
[42] Zelik, K. E., La Scaleia, V., Ivanenko, Y. P., and Lacquaniti, F., 2015, "Coordination of Intrinsic and Extrinsic Foot Muscles During Walking," Eur. J. Appl. Physiol., **115**(4), pp. 691–701.
[43] Voloshina, A. S., Kuo, A. D., Daley, M. A., and Ferris, D. P., 2013, "Biomechanics and Energetics of Walking on Uneven Terrain," J. Exp Biol., **216**(Pt. 21), pp. 3963–3970.
[44] Takahashi, K. Z., Kepple, T. M., and Stanhope, S. J., 2012, "A Unified Deformable (UD) Segment Model for Quantifying Total Power of Anatomical and Prosthetic Below-Knee Structures During Stance in Gait," J. Biomech., **45**(15), pp. 2662–2667.
[45] van Dieen, J. H., Spanjaard, M., Konemann, R., Bron, L., and Pijnappels, M., 2007, "Balance Control in Stepping Down Expected and Unexpected Level Changes," J. Biomech., **40**(16), pp. 3641–3649.